IEEE Trans. Image Processing, 2012.

A Unified Framework for Automated Iris Segmentation Using Distantly Acquired Face Images

Chun-Wei Tan, Ajay Kumar
Department of Computing, The Hong Kong Polytechnic University, Hung Hom, Hong Kong

Abstract: Remote human identification using iris biometrics has high civilian and surveillance applications and its success requires the development of robust segmentation algorithm to automatically extract the iris region. This paper presents a new iris segmentation framework which can robustly segment the iris images acquired using near infrared *or* visible illumination. The proposed approach exploits multiple higher order local pixel dependencies to robustly classify the eye region pixels into iris or non-iris regions. Face and eye detection modules have been incorporated in the unified framework to automatically provide the localized eye region from facial image for iris segmentation. We develop robust post processing operations algorithm to effectively mitigate the noisy pixels caused by the misclassification. Experimental results presented in this paper suggest significant improvement in the average segmentation errors over previously proposed approaches, *i.e.*, 47.5%, 34.1% and 32.6% respectively on UBIRIS.v2, FRGC and CASIA.v4 at-a-distance databases. The usefulness of the proposed approach is also ascertained from recognition experiments on three different publicly available databases.

1. Introduction

Iris recognition has been emerging as one of the most preferred biometric modalities for automated personal identification. Conventional near infrared (NIR) based iris recognition systems are designed to work in strictly constrained environments in order to mitigate the influence of the noises from various sources such as illumination changes, occlusions from eyeglasses, eyelashes, hair and reflections, just to name a few. The operating wavelength of the NIR used in such conventional systems is usually between 700-900nm, which has been used to reveal iris texture and provide sufficient contrast[*] even for the darkly pigmented irises. NIR illumination must be used with precaution and complied with the safety regulations. Excessive level of the NIR illumination can cause permanent damage to human eyes as the nature` of our

[*] The spectral radiance of human iris peaks at visible wavelength illumination. However the darkly pigmented iris often requires high level of intensity in visible illumination which can cause discomfort to the subjects.

human eyes is not instinctively responsive to the NIR illumination. Therefore, the iris images are usually acquired within a short distance between 1-3feet as the longer distances requires stronger NIR illumination, which may pose harmfulness to our eyes [1], [2], [4], [5].

Fig. 1. Sample iris images acquired in unconstrained environments.

There have been some promising efforts to acquire iris images using visible illumination to overcome the limitations of current iris recognition systems using NIR-based acquisition and develop less cooperative iris recognition systems for higher security and surveillance applications. The use of visible wavelength (VW) imaging can address the shortcomings of acquisition using NIR-based imaging, especially when distant acquisition for iris images is required. The advanced imaging technologies, for example, high resolution CMOS/CCD cameras, are now available to conveniently acquire high resolution images at distances beyond 3 meters using visible illumination and locate iris images suitable for recognition. Conventional iris recognition systems operate in stop-and-stare mode which requires significant cooperation from the users. The usage of visible imaging can relax such requirement and enable iris recognition in less cooperative environment using images acquired at further distance. Such iris recognition system can be a good candidate for high security surveillance such as identifying suspected criminals from the crowd [4]. References [3], [6] are two typical examples of the iris databases acquired using visible imaging which are now available in the public domain to promote further research efforts in this area.

Iris images acquired using unconstrained visible imaging is significantly noisier than those acquired by the conventional[†] iris recognition systems in the controlled environment. There can be multiple sources of commonly observed noise in such images and common ones may result from blurring artifacts caused by motion/defocus, occlusions from eyelashes, hair and eyeglasses, specular reflections, off-angles and partial images. Table 1 attempts to comparatively

[†] We refer to the iris imaging in controlled/constrained environments using NIR illumination.

summarize the iris recognition *at-a-distance* using VW and NIR imaging[‡]. Fig. 1 presents some noisy iris images which were acquired using visible imaging in unconstrained environments.

Table 1. Comparative summary of iris recognition 'at-a-distance' with different imaging conditions.

	Visible wavelength	**NIR wavelength**
Performance	Low	High
Applications	Forensics, surveillance	Commercial, high security
Imaging cost[§]	Low	High
Image quality	Degraded due to noise	Good
Medical/health concern	Low	High
User cooperation	Low	High
Key challenges	**Robust iris segmentation, iris feature extraction**	Segmentation and recognition are quite matured

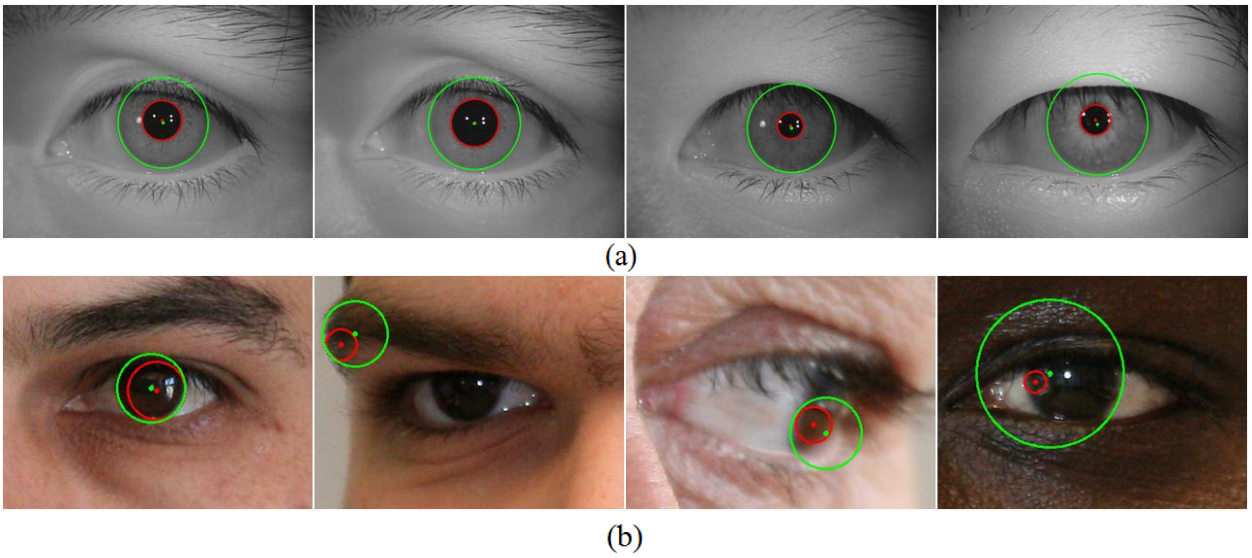

Fig. 2. Samples segmentation results from the conventional iris segmentation approach applied on (a) NIR acquired and (b) VW acquired iris images.

Integro-differential operator [2] is perhaps the most widely used iris segmentation approach deployed in most of the commercial iris recognition systems. The operator and its variants have shown effectiveness to segmenting the iris images for NIR acquired iris images in

[‡] The imaging cost not only includes the cost of the camera but also includes the cost of acquisition setup (for example, NIR illumination panels, bandpass filter, *etc*. [45]).

[§]

controlled environments [2], [7]-[10]. The operator works effectively when there is a significant contrast at the boundary of interest. There is typically more contrast at the pupillary boundary in NIR images than in visible light images. The conventional segmentation approaches often fail in segmenting the iris images acquired using visible imaging as the contrast level is degraded in those images. This failure can also be observed from the sample segmentation results in Figure 2(b) obtained by applying the conventional iris segmentation approach [2] on the iris images acquired under visible illumination. In addition, significant variations in pose, expressions[**] and illuminations, which are more common in unconstrained imaging environment, pose other significant challenges for the conventional iris segmentation approaches in effectively localizing the pupil and iris boundaries. Therefore, there is pressing needs for developing new image segmentation strategies, which are reliable and robust for automatically segmenting non-ideal iris images acquired using under visible illumination in the unconstrained or less constrained imaging environments.

The algorithm reported in [12] has been ranked the best in NICE.I (Noisy Iris Challenge Evaluation – Part I), which was the competition for the segmentation of noisy iris images acquired using visible imaging [13]. The algorithm first clusters the image pixels into two regions: skin and iris regions. The two clusters are initialized by using the top *M%* of the brightest pixels and top *N%* of the darkest pixels as the initial regions. The unassigned pixels are then clustered into corresponding region by calculating the point-to-region distance and by checking the 8-connecitivity to the region. The coarse iris location can be estimated based on the clustering result. The pupillary and iris boundaries are localized based on a integro-differential constellation model, which is a sub-optimal approach to the [2], [7] to speed up the algorithm. The effectiveness of the integro-differential constellation model investigated in this work is limited by several factors. Firstly, the parameters *M* and *N* must be carefully selected to avoid the over represented of the initial iris and skin clusters. The confusion will affect the segmentation performance at the later stage. Secondly, the segmentation approach is operating based on the conventional segmentation approach, which the effectiveness is relying on the radial gradient

[**] The iris region may not be visible or only partially visible (covered by eyelid) due to some facial expressions.

information. Lastly, the stop-at-once strategy adopted in the integro-differential constellation may lead to the convergence at non-center point for iris/pupillary region.

Another promising approach was reported in [4] by using neural network to classify the image pixels. The presented approach consists of two sequential stages: 1) sclera and 2) iris training/classification stages. Both stages exploit the local color features from HSV and YCbCr color spaces of the image. In addition to the color features, the iris stage also depends on the intermediate output from the sclera stage known as proportion of sclera. The proportion of sclera serves as the features with respect to four directions (east, west, north, and south) to delimit the iris region. As such, there exists a dependency between iris and sclera stages, in which the performance of the iris stage is directly affected by the sclera stage. Fig. 3 shows two samples of the sclera features extracted from two different iris images based on the algorithm in [4]. The defined color spaces are claimed to be capable to maximize the contrast between sclera and the other surrounding eye regions. However, our observations show that the discriminating features may not be stable for some images, as illustrated in Fig. 3(b). As compared to Fig. 3(a), much of the information contained in the hue component is not available. Also, the contrast between the sclera and iris regions in Cb (blue chroma) and Cr (red chroma) components are not contributing discriminative features as well. The deficiency of the discriminative sclera features will have the direct impact to the performance of the iris stage.

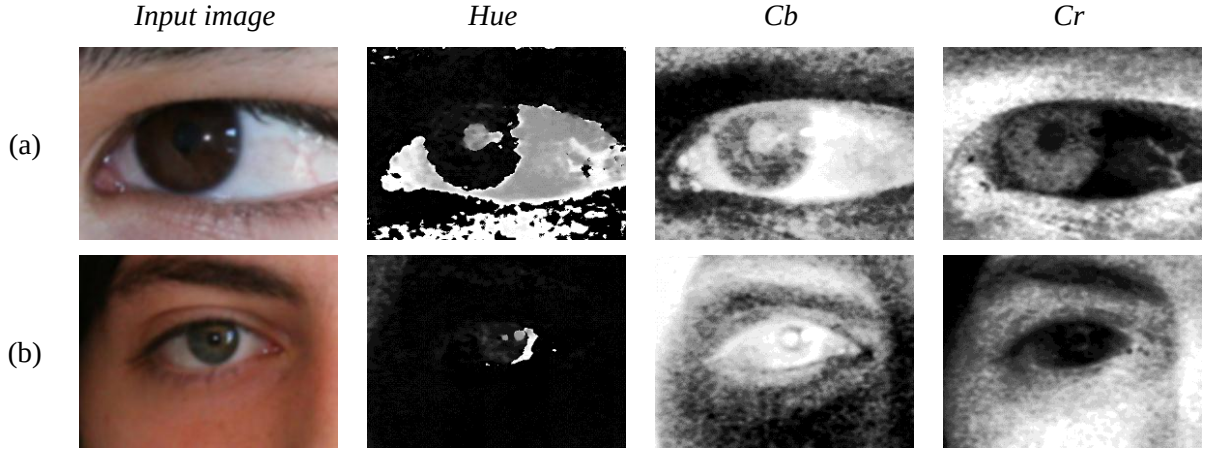

Fig. 3. Extracted sclera features with (a) high and (b) poor discrimination with iris region.

1.1 Our work

Remote identification of human at-a-distance using iris biometrics requires development of completely automated algorithm which can robustly segment the iris region from the distantly

acquired facial images. Despite some initial efforts in segmenting the VW iris images acquired in unconstrained conditions, the segmentation accuracies of those methods are quite limited. This paper focuses on the aforementioned segmentation problem and develops a completely automated and unified approach to segmenting the iris region from the facial image at a distance acquired using VW and NIR imaging [37]. The proposed approach works at pixel level by exploiting the localized Zernike moments [14] at different radii to classify each pixel into iris or non-iris category. Zernike moments have been shown to constitute discriminant features for the image representation since they are less sensitive to noise and the information redundancy. The complete orthogonal and rotation invariance properties of the Zernike moments are effectively exploited in the proposed segmentation approach for the noisy iris images acquired under visible illumination in unconstrained environments. The scale invariance in the feature representation is inherently addressed during the mapping process from a localized iris region to a unit circle. One of the important features of the proposed iris segmentation approach is its ability to segment iris images acquired under varying illumination bands and therefore offers a *unified* solution for the iris segmentation. Unlike previous approaches on VW iris segmentation, the proposed segmentation strategy for VW iris images is seamlessly adapted for NIR images and does not require any modification to segment iris images under variable spectral bands. In order to compensate the misclassification of the image pixels due to the limitations of the classifier, we develop a set of post-classification operations (Section 2.2) to robustly mitigate the influence of such noisy pixels (non-iris pixels). The post-classification processing is shown to be highly effective in reducing the segmentation error. Rigorous experiments were performed on two kinds of publicly available databases: (1) databases with localized face images (FRGC [21] and CASIA.v4 iris-at-a-distance (hereafter referred as CASIA.v4-distance) [31]) and (2) database with localized eye regions (UBIRIS.v2 iris database [3]). On the first case, face region is automatically localized by using AdaBoost-based face detector followed by a AdaBoost-based eye pair detector to localize the eyes. The performance comparison between the neural network and support vector machine based classifiers using the segmentation method is reported from the extensive experiments to ascertain the adaptability of the developed approach to different imaging environment/databases. The experimental results presented in this paper suggest an average improvement in the iris segmentation error by 47.5%, 34.1% and 32.6%, respectively on publicly available UBIRIS.v2, FRGC and CASIA.v4-distance databases, as compared to those

from previous approaches [4], [12], [10]. One of the important aspects of the experimental results and comparison presented in this paper is related to their repeatability. We have provided all the details of the employed images from the respective databases in our experiments (to ensure repeatability of experiments) and all the ground truth images employed in our evaluation [43]. In addition, recognition performance is also evaluated in order to ascertain the usefulness of the distantly acquired images for robust human recognition.

The remainder of this paper is organized as follows. In Section 2, the proposed unified segmentation approach and the post-classification processing operations are detailed. The experiments and performance evaluation are presented in Section 3. Finally, discussions and conclusions are provided in Section 4.

2. Iris segmentation for images acquired in visible and NIR illumination

The iris segmentation approach developed in this paper is motivated by the work in [4]. The segmentation approach adopts pixel-based strategy to classify each pixel into iris/non-iris category. Fig. 4 and 5 show the block diagrams of the proposed iris segmentation approach for both localized eye and face images. The proposed segmentation approach can be divided into two stages: 1) training/classification and 2) post-classification. In the training/classification stage, local information at each image pixel is extracted by exploiting the Zernike moments represented by different radii. For training, the extracted localized Zernike features and the desired output labels (manually labeled iris mask) are fed into the machine learning algorithms such as neural network (NN) and support vector machine (SVM). For classification, the

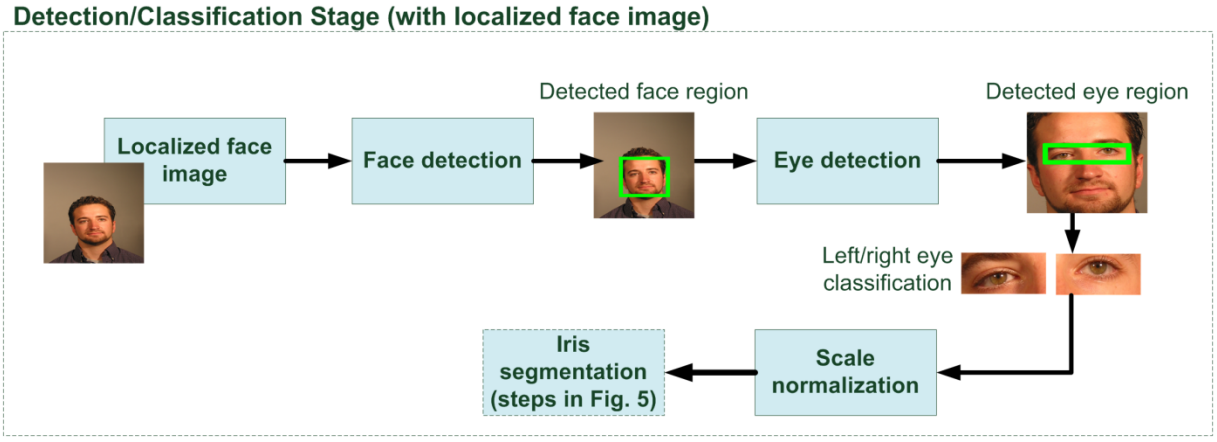

Fig. 4. Block diagram of the proposed iris segmentation method with localized face image.

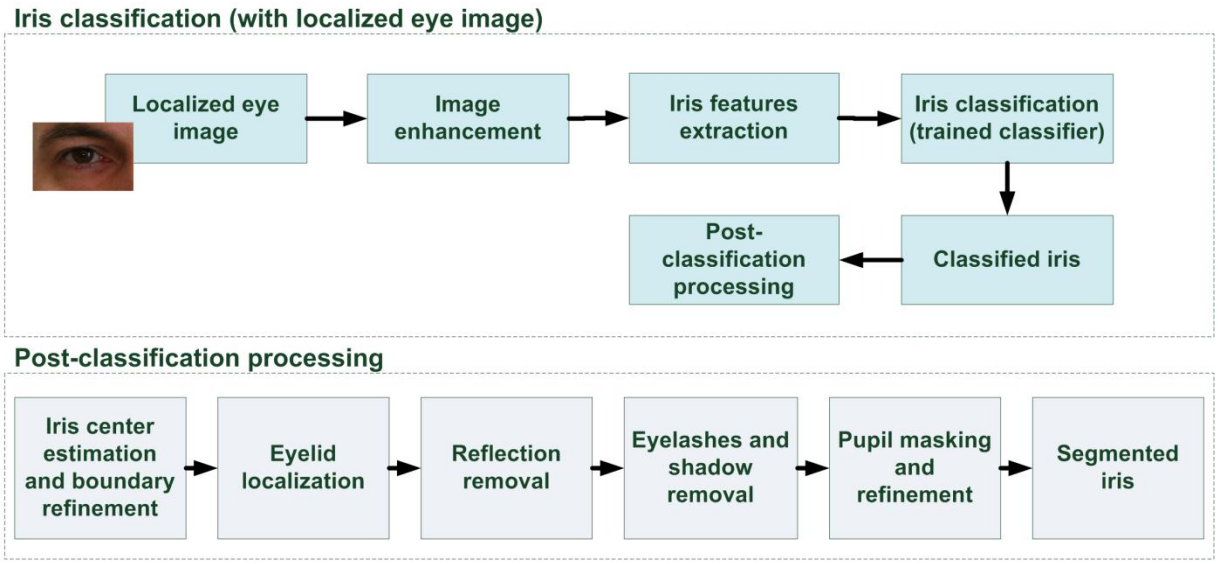

Fig. 5. Block diagram of the proposed iris segmentation method with localized eye image.

extracted Zernike features are passed to the trained classifier to predict the labels for each of the image pixel. Due to the limitations of the classifier, the classified output may contain some misclassified pixels which are not part of the iris region. As such, simple image processing techniques such as the morphological operations can be applied to eliminate majority of the non-iris pixels. In this work, a set of post-classification processing operations are developed (section 2.2) to further complement the trained classifier, in order to further refine the classified output. The post-classification processing operations are shown to be highly effective to further reducing the average segmentation error.

2.1 Detection/Classification

2.1.1 Face and eye detection

Automated segmentation of eye region images, from the given face images in our experiments, is illustrated in Fig. 6. A hierarchical detection strategy is adopted by firstly detecting the face region. An eye- pair detector is then applied on the localized face region. The hierarchical detection approach improves the robustness to detect the eye region by confining the region of interest at each level, as compared to apply a single eye-pair detector. In this work, AdaBoost-based face and eye-pair classifiers are employed for face and eye detection [22], [23]. The resulting output from the AdaBoost-based eye-pair detector is further refined by classifying each

eye into left or right eye category. The left or right eye classification is simply partitioning the width of the detected eye-pair region, the first half as right eye and the second half as left eye.

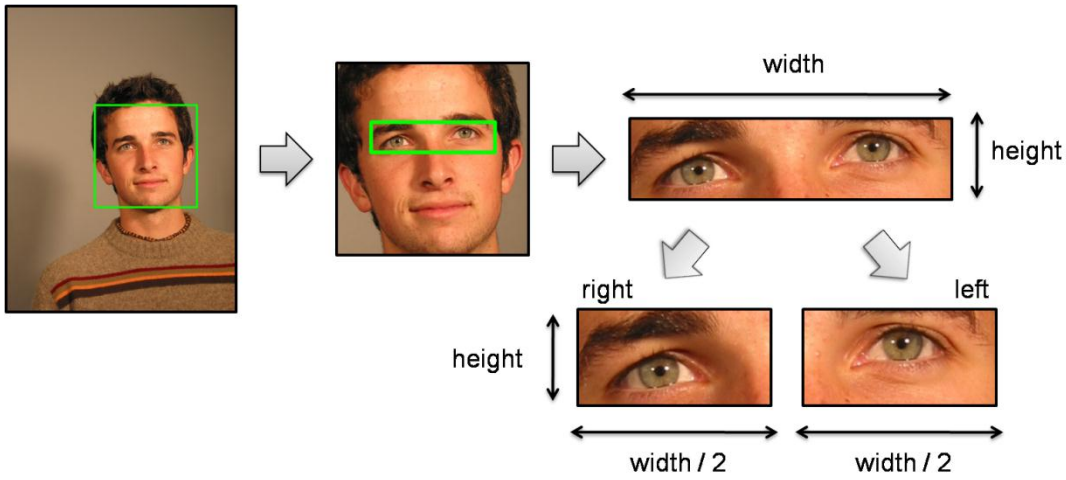

Fig. 6. Hierarchical face-eye detection.

2.1.2 Image enhancement

Illumination variation poses the difficulties for both iris segmentation and recognition. The influence of the illumination conditions is even more noticeable when the acquisition is performed in the unconstrained environments using visible imaging. The problem, although usually been addressed, none of the approaches provide the solution especially in the context of

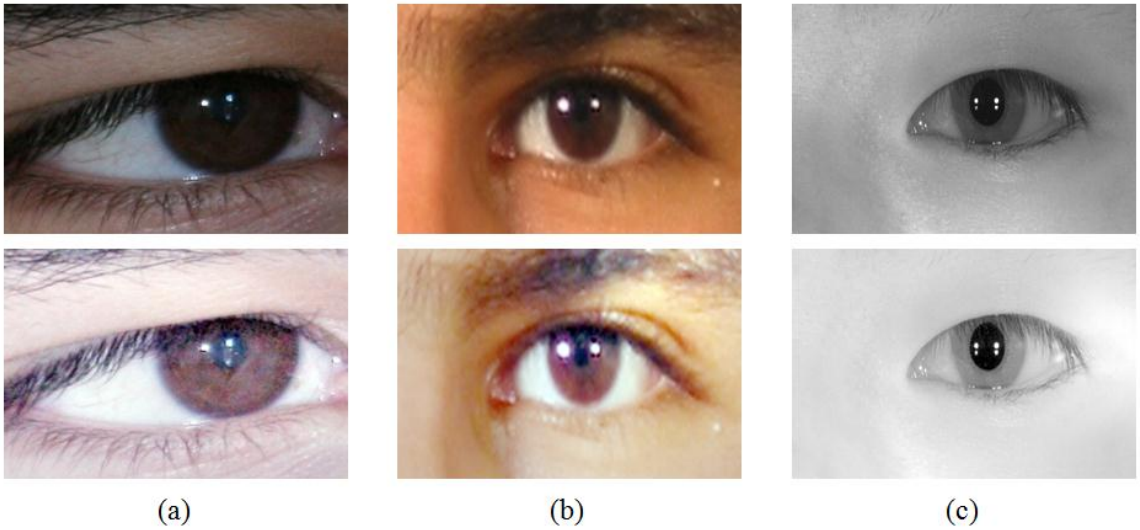

Fig. 7. Image enhancement using SSR, image samples from (a) UBIRIS.v2, (b) FRGC, (c) CASIA.v4-distance.

iris segmentation for images acquired in the unconstrained environments using visible imaging [2], [10], [19], [34], [35]. For that reason, we propose to take the advantages of Single Scale

Retinex (SSR) algorithm for improving color consistency regardless of illumination variation [28]-[30]. The mathematical form for the SSR is as follows:

$$R_{i\in\{R,G,B\}}(x_1, x_2) = \log \frac{I_i(x_1, x_2)}{G_\sigma * I_i(x_1, x_2)} \tag{1}$$

where I_i denotes the input image with i channels, G_σ denotes the Gaussian kernel with standard deviation σ and '*' denotes the convolution operator. For the case of NIR images, the multispectral channels are reduced to gray level. The SSR is applied on the localized eye region for image enhancement prior to the feature extraction operation. Fig. 7 shows some samples of the SSR enhanced images *R* from the three databases employed in the experiments.

2.1.3 Feature extraction

Localized texture description based on Zernike moments (ZM) has been shown to outperform other alternatives in terms of noise resilience, information redundancy and image representation [14], [15], [24], [25]. Therefore ZM is used as the feature extractor to compute higher order local pixel dependencies in the local region. We extracted six features for every pixel at location (x_1, x_2) from a given image I in the local region represented by multiple radii. The computed feature vector is of 6-dimensional defined as follows:

$$\{x_1, x_2, I(x_1, x_2), Z^l_{mn}(I, x_1, x_2)\} \tag{2}$$

where I represents single channel of enhanced eye image. Therefore, conversion of the color image to the single channel image is required, for example, the images acquired using visible imaging. In order to meet such requirement, the red channel of the color image is employed[††]. This particular channel is utilized due to its spectral proximity towards NIR wavelength, which is commonly employed to acquire discriminative iris feature [12]. The Z is a function of I centered at (x_1, x_2) which used to calculate the ZM at radius $l \in \{2, 5, 7\}$. The ZM of order $m \in \mathbb{N}$ (m) and repetition $n \in \mathbb{Z}$ can be calculated using equation (3).

$$Z^l_{mn} = \frac{m+1}{\pi} \sum_{x=x_1-l}^{x=x_1+l} \sum_{y=x_2-l}^{y=x_2+l} f(x, y)\left[V_{mn}(r, \theta)\right]^* \tag{3}$$

[††] The red channel image is employed throughout the experiments.

The Zernike order *m* is respectively set to 4 and 6 for VW and NIR databases and the repetition *n* is set to zero for databases from both wavelength[‡‡]. The function *f* denotes the extracted local region/sub-image which is mapped to a unit circle, i.e., $(x^2 + y^2 \leq 1)$. The Zernike polynomials *V* across the radius $r \in [0,1] : r \in \mathbb{R}$ in the polar form is

$$V_{mn} = R_{mn}(r)e^{in\theta} \tag{4}$$

where the repetition term *n* is subject to the conditions such that, $m - |n|$ is even and $|n| \leq m$. The radial term in (4) is given as

$$R_{mn}(r) = \sum_{s=0}^{(m-|n|)/2} (-1)^s \frac{(m-s)!}{s!\left(\frac{m+|n|}{2} - s\right)!\left(\frac{m-|n|}{2} - s\right)!} r^{m-2s} \tag{5}$$

2.1.4 Training and classification

The goal of classification is to find a generalized solution which can optimally separate the data into their corresponding classes/categories. SVM offers a computationally simpler model to obtain the solution which is global minimum and unique, as compared to NN. However, the performance comparison of each algorithm to solve the classification problem for iris segmentation has not yet been reported. In this work, two commonly used supervised machine learning approaches: feedforward neural network (FNN) and SVM are evaluated in order to show the adaptability to each different database used in our experiments. Both the classifiers are trained with the same training images, which are independent from the test images. Features are extracted for each image pixel which forms a set of feature vectors according to (2). As the supervised learning approaches require the labels (desired outputs) to be provided, iris regions of all the training images are manually masked to generate the binary labels. Fig. 8 shows some samples of the training images from each different database and the corresponding manually labeled iris masks. It is important to note that the sample images shown in Fig. 8 are for illustration only and all the images employed are subject to the processing as described earlier. The extracted features from all the training images contribute a large amount of positive (iris) and negative (non-iris) training samples. However, only fraction of the positive and

[‡‡] The coefficients were chosen empirically using training samples which were independent from the test dataset.

negative samples up to a certain amount is randomly selected to be used for training.

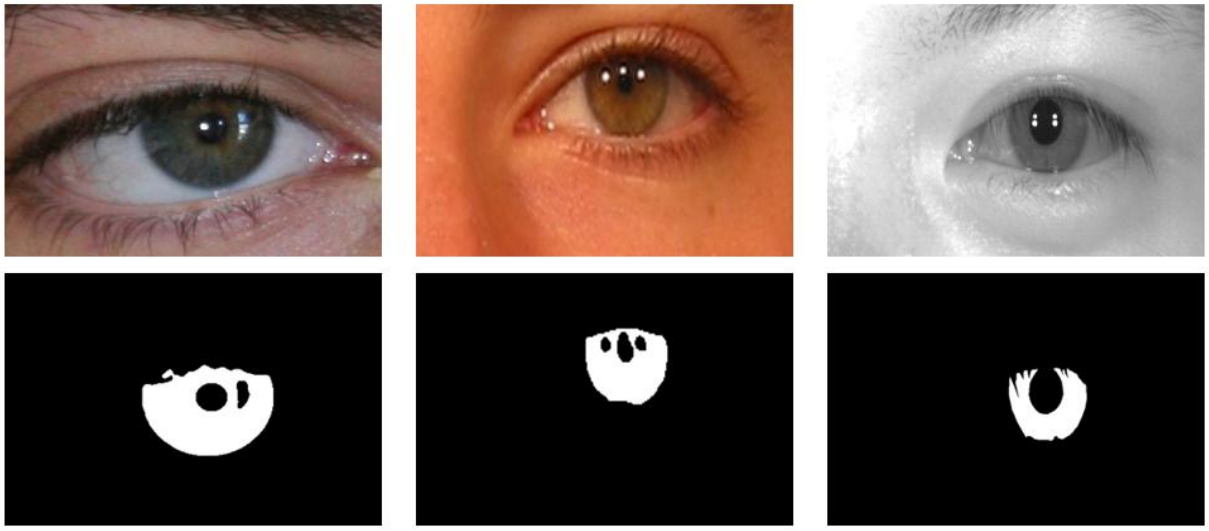

Fig. 8. Sample training images and the corresponding manually labeled masks from database (a) UBIRIS.v2, (b) FRGC, and (c) CASIA.v4-distance.

The information used in learning for both FNN and SVM are summarized in Table 2 and 3, respectively. For FNN, back-propagation with Levenberg-Marquardt learning method [26] is employed. Network topology selected in the experiments is a typical 3-layer FNN which consists of an input layer (i), a hidden layer (h) and an output layer (o) denoted as $N_i - N_h - N_o$ in Table 2, where N_β indicates the number of neurons at layer $\beta \in \{i, h, o\}$. For SVM, radial basis function (RBF) is selected as the non-linear kernel based on the preliminary results obtained from the validation samples. Table 3 suggests that least amount of positive and negative training samples[§§] are used for training the SVM classifiers as compared to FNN. The differences are due to the fact that the generalization performance of an SVM is less dependent on the training data and is fully determined by the support vectors [27]. Classification of iris pixels is performed by using the trained classifier as described above. Features are extracted for each pixel in a similar manner as in learning phase to form a collection of feature vectors. The set of feature vectors is fed into the trained classifier to induce labels (iris/non-iris) for each pixel.

[§§] Training samples used to train the SVM classifiers are subset of the training samples employed to train the NN classifiers.

Table 2. Training configurations for FFN-based classifiers.

	UBIRIS.v2	FRGC	CASIA.v4-distance
Total number of train images	41	40	41
No. of features per pixel	6		
No. of +/- samples	25000 / 25000		
No. of layes and neurons	6-11-1	6-11-1	6-9-1
Radii for windows (pixels)	2, 5, 7		
Order of Zernike Moments	4		6
Learning algorithm	Levenberg-Marquardt		

Table 3. Training configurations for SVM-based classifiers.

	UBIRIS.v2	FRGC	CASIA.v4-distance
Total number of train images	41	40	41
No. of features per pixel	6		
No. of +/- samples	10000 / 10000	10000 / 10000	10000 / 10000
Radii for windows (pixels)	2, 5, 7		
Order of Zernike Moments	4		6
Kernel function	Radial Basis Function (RBF)		

2.2 Post-classification processing

The operations developed in this section play a vital role to further refine the classification results produced by the trained NN/SVM classifier. The pixels classified by the trained NN/SVM classifier often include noise resulting from false negative and false positive errors in the classification stage. Therefore, the robust post-classification processing steps are developed to mitigate the errors and improve the segmentation accuracy of the algorithm.

2.2.1 Iris center estimation and boundary refinement

Iris center is estimated by fitting a circle to an edgemap generated using the classified iris mask which is firstly processed with morphological operations. The holes (pupil/reflection in the classified iris masks) are filled to obtain better estimation of iris center by minimizing the influence from the pupil and reflection regions. There are two parameters required for the operation: i) initial iris center and ii) range of radius, which both can be easily

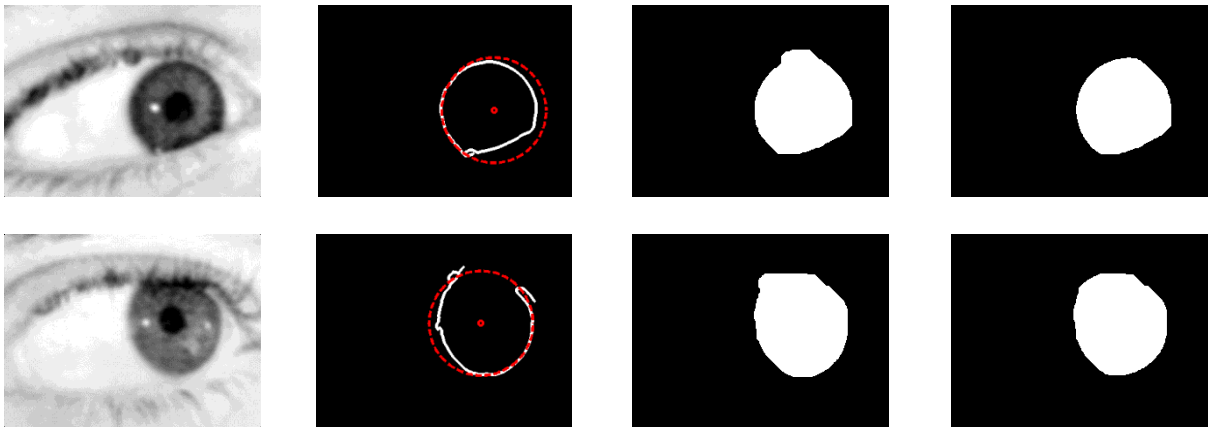

Input image ***Estimated iris center*** ***Classified iris mask* (*with morphological operations*)** ***Refined iris mask***

Fig. 9. Examples of iris center estimation and boundary refinement.

estimated from the classified binary iris mask *B*. The initial center (C_{x1}, C_{x2}) is estimated by calculating the center of mass of the *B*. For estimating the range of radius *r*, one can utilize the width and height information of *B*. In this work, we consider only the height information *h*, which is least sensitive to the presence of eyelashes spread horizontally. The *r* can be computed as follows:

$$\{r \in \mathbb{N} : \alpha h \leq r \leq \beta h, \alpha, \beta \in \mathbb{R}, \alpha \leq \beta, \alpha, \beta > 0\} \quad (6)$$

After obtaining the necessary parameters, the best fitted circle is searched within a small offset (±15 pixels) from the (C_{x1}, C_{x2}). The pixels in *B* which are fallen outside the best fitted circle are removed, resulting in a boundary refined iris mask, as shown with some examples in Fig. 9.

2.2.2 Eyelid localization

The estimated iris center (C'_{x_1}, C'_{x_2}) and the radius *r* obtained in the previous step are employed here. The iris center serves as a reference point to partition the localized iris into two regions: upper and lower eyelid regions, which are delimited by *r*. Both upper and lower eyelids can be localized in a similar manner, thus we explicate the localization approach by using the upper eyelid as an example. The key idea of the eyelid localization is to fit a polynomial curve with degree 2 to the candidate eyelid points extracted from an edgemap generated using Canny edge detector [32]. Considering the fact that the intensity of eyelashes is usually darker than the skin

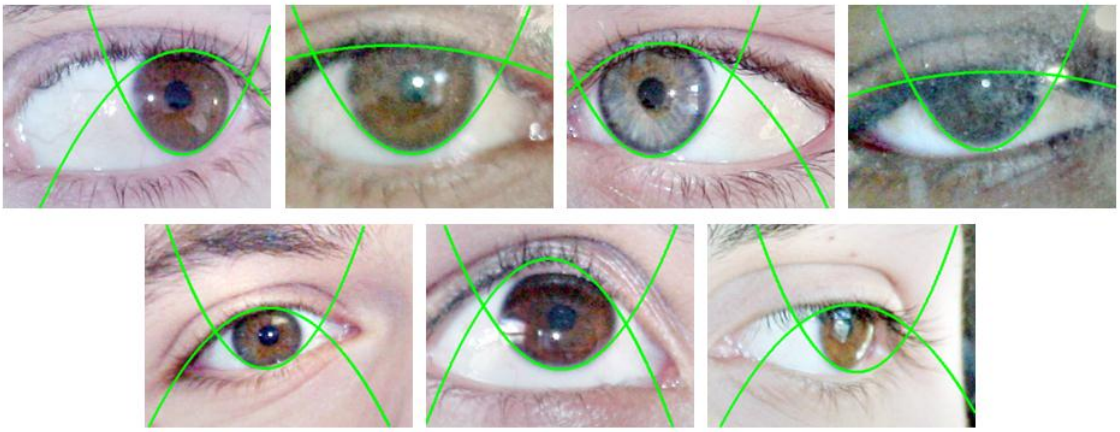

Fig. 10. Sample eyelid localization results for iris images with various noisy artifacts.

and iris regions, robustness to extract the candidate eyelid points can be improved by exploiting the intensity information of an input image *I* simultaneously. The average columnwise intensity information, $\mu_1$and μ_2, delimited by *P* pixels from an edge point (E_{x_1}, E_{x_2}), i.e.

$$\mu_1 = \frac{1}{P}\sum_{x_2'=x_2-P}^{x_2-1} I(E_{x_1}, E_{x_2'}) \quad ; \quad \mu_2 = \frac{1}{P}\sum_{x_2'=x_2+1}^{x_2+P} I(E_{x_1}, E_{x_2'})$$

are computed. The (E_{x_1}, E_{x_2}) is considered a rightful candidate if $\mu_1, \mu_2 > I(E_{x_1}, E_{x_2})$ is satisfied. Furthermore, we adopted the strategy in [19] to consider only one edge point per columnwise, which can further mitigate the effect from the outlier. Fig. 10 presents some sample of the eyelid localization results which has shown superior performance even under challenging conditions.

2.2.3 Reflection removal

Reflection removal technique reported here can be considered an extension to [19]. In [19], an adaptive threshold is calculated by considering the top 5% of the brightest intensity[***] of an image. The calculated threshold is used to extract the candidate reflection regions. The extracted regions are filled using bilinear interpolation method. The reflection problems appear to be more challenging in unconstrained environments for visible imaging acquisition images due to multiple sources of the reflections (specular and diffuse). In addition, the levels of pigmentation also quantify the spectral radiance in the iris region, from which the variation is more significant

[***] The percentage reported was tuned for NIR acquired iris images.

in visible imaging [4], as depicted in Fig. 11. The dynamic nature of the reflection in visible imaging acquired images justifies that the reflection removal technique in [19] is not sufficient for capturing the reflection regions in unconstrained environments. For that reason, we propose a relativity propagation reflection pixel detection approach, which can robustly localize the reflection regions. This approach can be detailed as follows:

Fig. 11. Reflection is often severe for the iris images acquired *at-a-distance* using VW imaging in *unconstrained* environments.

1. Candidate reflection regions are firstly initialized, similar to as in [19] by considering the top 20% of the brightest intensity as the candidate regions. The candidate regions which are fallen beyond the iris region are filtered and are not to be considered in the subsequent operations. The remaining candidate regions serve as seed points [†††] $\{\boldsymbol{s}_1, \boldsymbol{s}_{2,\cdots,}\boldsymbol{s}_n\}$ for the propagation to work. Select a relativity term $\{R \in \mathbb{R}: 0 \leq R \leq 1\}$, which is used to calculate the relative threshold.
2. Evaluate the 8-connected neighborhood pixels $N_{j=1,\cdots,8}(\boldsymbol{s}_i)\ of\ \boldsymbol{s}_i$ which is not indicated as reflection point. If the intensity value of $I(N_j) \geq R \times I(\boldsymbol{s}_i)$, mark N_j as reflection point and repeat 2 at N_j for p iteration (p is set to 5 throughout the experiments).

The undetected reflection points are propagated by comparing the intensity values with respect to the center pixel (reference pixel) in an 8-connectd neighborhood, whose relationship is controlled by the relativity term R[‡‡‡]. For examples, let R = 0.9, the neighborhood pixels whose

[†††] One can opt for other methods to initialize the seed points.

[‡‡‡] 90% – 95% intensity value from the reference pixel is a reasonable choice for parameter R.

intensity value is of 90% of the reference pixel is then updated as reflection point. Figure 12 presents the sample results for reflection detection using [19] and the proposed method.

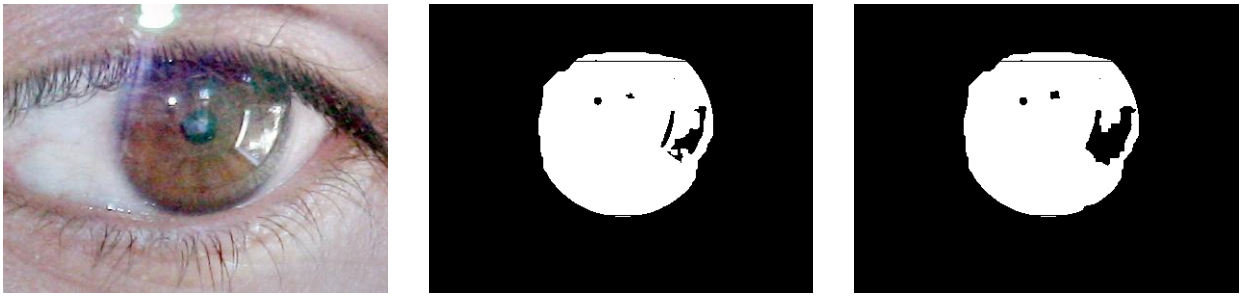

(a) (b) (c)

Fig. 12. Reflection detection; (a) source image (b) method [19] (c) proposed method.

2.2.4 Eyelashes and shadow removal

The proposed eyelash and shadow removal approach is motivated based on [19] by exploiting the intensity distribution of the classified/localized iris region, as illustrated in Fig. 13. The localized iris region is first divided into two sub-regions namely eyelashes and shadow (ES) region, and iris (IR) region, as depicted in Fig. 13(a). The ES region is defined as the area from the upper eyelid delimited by distance d with respect to the iris radius r_{ir}, i.e. $(d = r_{ir} \times 0.3)$. Histograms of these sub-regions are constructed subject to the transformation as follows:

$$G(i) = e^{\frac{(H(i)-H_{\mu})^2}{2H_{\sigma}^2}} \tag{7}$$

where i denotes the intensity level, H_{μ} and H_{σ} denote the mean and the standard deviation of the histogram H. An adaptive threshold τ_{es} to mask out the noisy artifact in ES region can be obtained by considering the intensity levels I_{peak_es} and I_{peak_ir}, from the peaks of the transformed histograms, i.e. $\tau_{es} = \delta \times \left(I_{peak\_es} + I_{peak\_ir}\right)$. The δ can be considered as a weight that bias to either side of the peak, which is set to 0.4 for all of the experimental results reported in this paper.

2.2.5 Pupil masking

Accurate localization of the pupil region for VW acquired images is more challenging as compared to those for NIR acquired images. This problem becomes more serious for the darkly pigmented irises where the contrast level between pupil and iris regions is relatively low. The

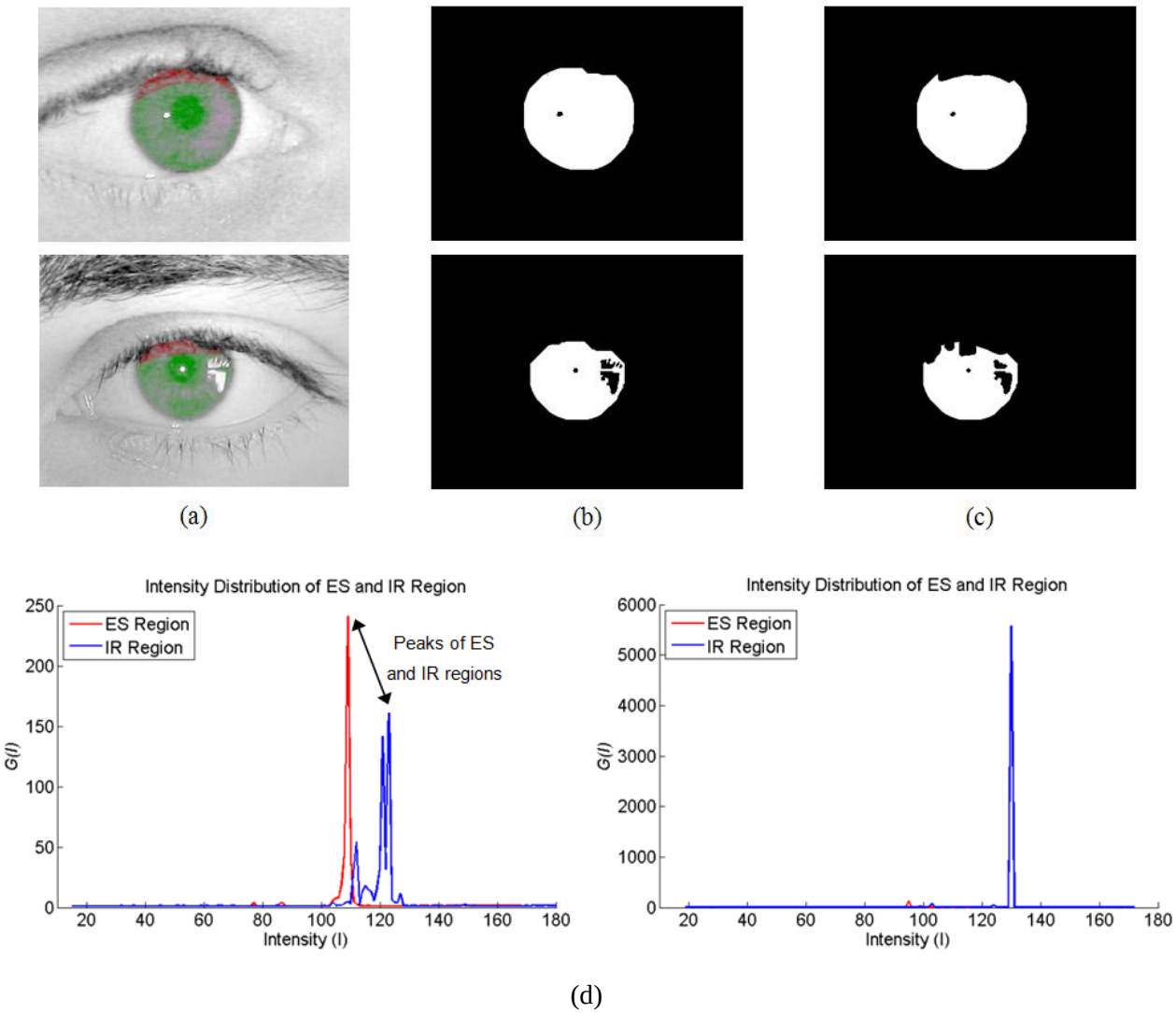

Fig. 13. Eyelashes and shadow removal; (a) ES (red) and IR (green) regions, (b) localized iris masks before ES removal, (c) localized iris masks after ES removal (d) histograms of sub-regions of images in (a).

image enhancement technique described in section 2.1.2 plays an important role to address such problem. This can also be observed from the images in Fig. 7 where the contrast level between pupil and iris regions is greatly improved after applying the retinex algorithm for image enhancement. In order to localize the pupil region, the gray level distribution in the localized iris

region is again exploited to automatically compute the adaptive threshold τ_p to extract the candidate pupil region, i.e. $\tau_p = \alpha \times (\varphi(H_{max}) + \varphi_0)$. The function φ returns the intensity level of the maximum frequency H_{max} of the histogram and φ_0 denotes the minimum intensity level from the histogram. The constructed histogram is divided into 10 equally spaced bins as we assume the intensity values in the localized iris region are highly similar since most of the artifacts such as reflection, eyelashes and shadow have been eliminated with the prior post-processing operations.

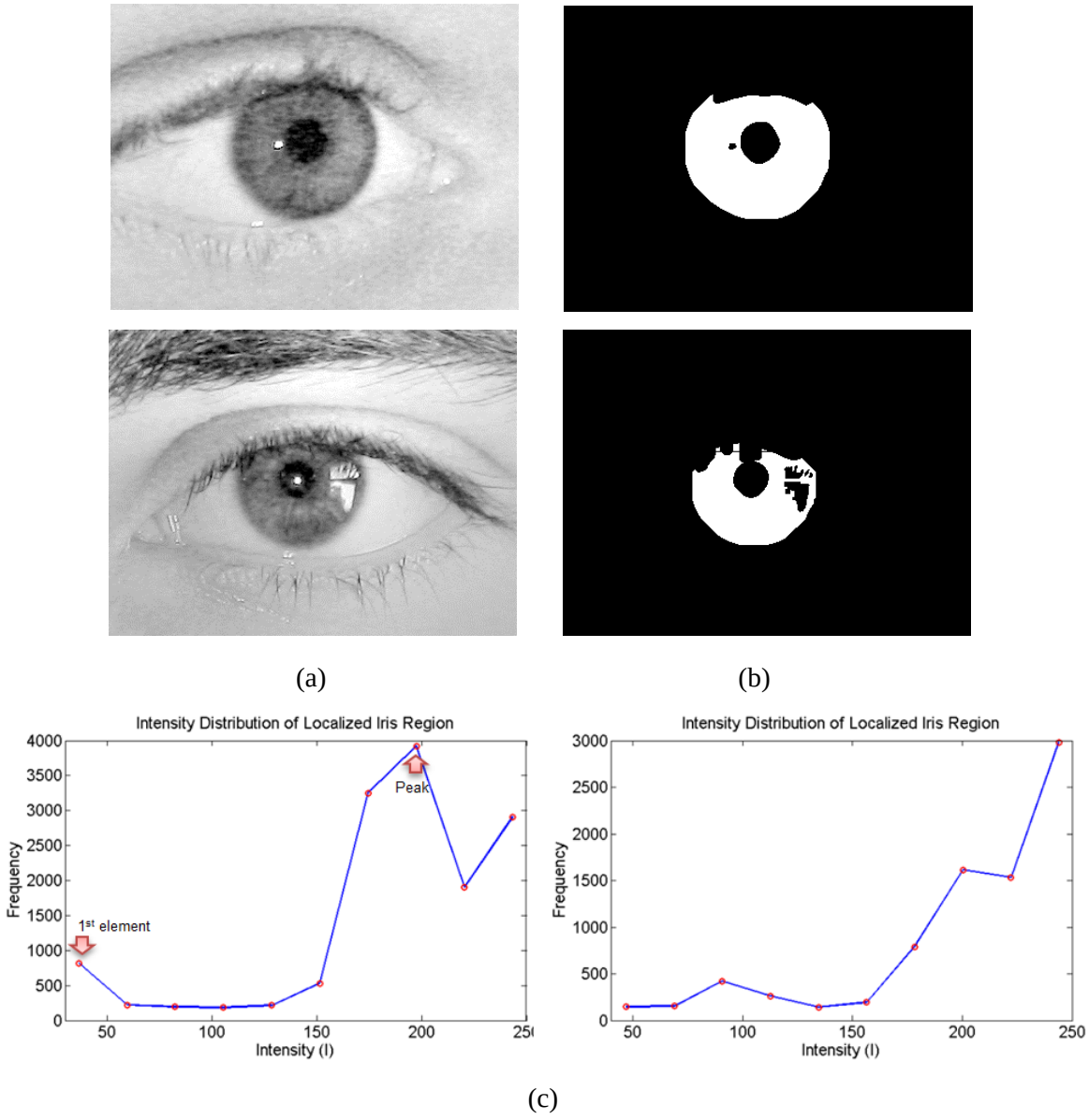

Fig. 14. Pupil localization; (a) input images, (b) binary masks after pupil masking, (c) histograms of the localized iris regions for images in (a).

The parameter α can be considered as a weight factor which determines the τ_p, which is set to 0.4 in all the experiments. The selection of τ_p is motivated by the fact that the intensity distribution for iris pixels is more concentrated (peak of the histogram) in the localized iris region. The extracted candidate pupil region is subjected to the refinement using morphological operations and pupil center can be approximated similar to the steps for finding iris center, as described in section 2.2.1. Fig. 14 illustrates sample pupil localization results using the approach described in this section.

3. Experiments and results

In order to ascertain the performance of the proposed unified segmentation approach for distantly acquired iris/face images, experiments on three free publicly available databases: UBIRIS.v2, FRGC and CASIA.v4-distance were utilized. The first two databases were acquired using visible imaging while the latter was acquired using NIR imaging. All the databases employed in the experiments provide the images acquired at a distance ranging from 3 – 8 meters[§§§], which have justified the main objective of our work. Repeatability and reproducibility of the experimental results are one of the important issues in biometrics. It is not uncommon for the researchers to find difficulties in reproducing the published results due to lack of details on the selection of training/test images, especially in the context of visible imaging iris recognition. We have therefore elaborated such desired information to ensure reproducibility of experimental results.

Table 4. Summary of the train/test images from different databases employed in the experiments

	UBIRIS.v2	**FRGC**	**CASIA.v4-distance**
Imaging type	VW	VW	NIR
Standoff distance	4 – 8 meters	N/A	≥ 3 meters
No. of test images (S/R)	904 / 904	500 / 500	502 / 961
No. of test subjects (S/R)	152 / 152	150 / 150	67 / 131
No. of train images (S/R)	40 / 96	40 / 40	41 / 79
No. of train subjects (S/R)	17 / 19	13 / 13	6 / 10

[§§§] The exact standoff distance is not yet available for the still images in FRGC database.

Above table summarizes the respective details on the train/test images employed in two types of experiments performed in this work. The first type of experiment evaluates the segmentation accuracy from the proposed segmentation approach. The second type of experiment evaluates the recognition performance using the segmented iris images. The details for the segmentation and recognition experiments are denoted respectively as **S** and **R** in Table 4.

3.1 Databases

- ***UBIRIS.v2.*** The database is the contribution of the SOCIA Lab from the University of Beira Interior. The images were acquired in unconstrained conditions using visible imaging which presents more realistic noise factors. The full database consists of a total of 11102 images acquired from 261 subjects in two distinct sessions. The standoff distance of the subjects to the camera is range from 4 to 8 meters [3]. A subset of this database which consists of 1000 images from 171 subjects was employed in the experiments. This database subset was released for Noisy Iris Challenge Evaluation - Part II (NICE:II), which was a competition initiated from the same research team [20]. The first 96 (19 subjects) out of the 1000 images were selected as training samples. The remaining 904 (152 subjects) images were served as test samples.

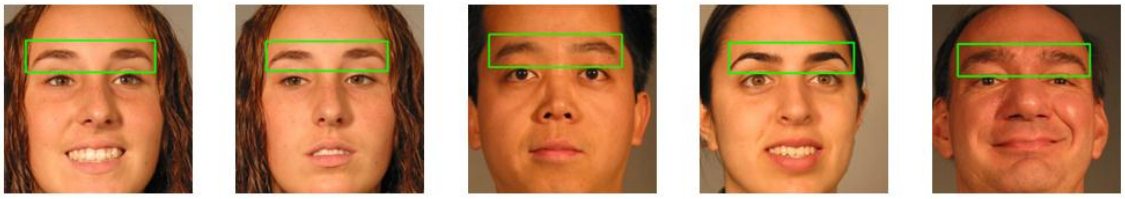

Fig. 15. Falsely classified eye-pair region by AdaBoost eye-pair classifier.

- ***FRGC.*** FRGC database was acquired to encourage the development and evaluation of new algorithms for automatic face recognition. The databases comprised of three categories of images: high resolution still images, 3D images and multi-images of a person [21]. Among the available categories, the high resolution still images were employed in our experiments as the images in this category can closely represent/meet the objective of our work. The images employed in the experiments were selected from the sessions **2002-269** to **2002-317** of "**Fall2002"** academic year. Eye regions were automatically extracted from the face using the procedures as described in section 2.1.1.

Our observations have suggested that the average iris diameter from the extracted eyes images are less than 140 pixels, which do not meet the minimum acceptable diameter as reported in [2]. The ISO/IEC 19797-6 Annex A [35] requires even stricter constraint on iris diameter with a minimum of 200 pixels for high security applications. Therefore, it is reasonable to filter or reject those images which are not expected to be compliant (or even near) with such standard. We have also estimated the average iris diameter for the segmented iris images for all the three employed databases, using the ground truth masks, and are summarized in table 5. As such, we applied filtering rule to the results obtained from the AdaBoost-based eye-pair classifier. The detected eye-pair regions not satisfying the predefined minimum size of 300 × 150 pixels were not considered in the experiments[****]. The qualified eye-pair region is subject to further classification into left or right eye region and rescaled the region size to 300 × 150 pixels. The AdaBoost-based eye-pair classification also has some limitations, though not serious, which remains to be addressed to ensure accurate eye-pair detection. The false alarm rate is 0.93%, for all the FRGC images considered in this experiment. The falsely classified eye-pair images (see Fig. 15) where not considered in the experiments.

Table 5: Estimated Iris diameters

	Min. diameter	**Max. diameter**	**Mean diameter**
UBIRIS.v2	49	200	122.48
FRGC	46	75	61.72
CASIA.v4-distance	129	185	164.23

- ***CASIA.v4-distance*.** The first publicly available long-range and high quality iris/face database acquired using NIR imaging released by the Center for Biometrics and Security Research (CBSR) from the Chinese Academy of Sciences (CASIA). The full database consists of a total of 2567 images acquired from 142 subjects in single session. The standoff distance of the subjects to the camera is from 3 meters away [31]. Images from the subject 1 to 10 were selected for training, while the rest serve for testing purpose (images from subject 11-77 used in experiment **S**; images from subject 11-141 used in

[****] Although the filtering rule provides localized eye images with larger iris diameters, the average iris diameter is still beyond the minimum requirement set by the ISO/IEC 19797-6.

experiment **R**). Note that only the first *eight left eye* images from each subject were employed in the experiments. Similarly to the FRGC database, eye region detection and classification are required in order to provide the localized eye image for segmentation. The false alarm rate of AdaBoost-based eye-pair classifier is 4.76%, for all the images employed in the experiment from this database.

3.2 Evaluation protocols and experimental results

Experiments were carried out on three publicly available databases to ascertain the performance of the proposed iris segmentation approach. In addition, recognition performance for the images from these three challenging databases was evaluated. The evaluation is essential to ascertain the usefulness of the distantly acquired images for robust human recognition. Both segmentation and recognition performance is also compared to three state-of-the-art methods [4], [12], [10], which were reproduced in either C/C++ (with OpenCV Library) or Matlab environment.

3.2.1 Experiments on segmentation (*S*)

In order to ascertain the performance from the proposed iris segmentation approach, the evaluation protocol as used in NICE.I competition [13] is adopted. The classification error *E* is employed as the performance criterion and can be expressed as follows:

$$E = \frac{1}{c \times r} \sum_{c'} \sum_{r'} O(c', r') \otimes C(c', r') \tag{8}$$

where *O* and *C* referring the ground truth and segmented iris masks; *c* and *r* denote the width and height of the image, respectively. The '⊗' denotes an XOR operator which evaluates the disagreeing pixels between the ground truth *O* and the segmented iris masks *C*. Table 6 and 7 summarize the segmentation results obtained from the proposed segmentation approach on the three databases described earlier as well as the comparisons with the state of the art methods [4], [12], [10]. The proposed method has achieved improvement of 49.3% and 45.6% on UBIRIS.v2 database over the methods [4] and [12], respectively. For the experiments on FRGC database, improvement of 24.0% and 44.2% has been achieved as compared to [4] and [12]. The improvement of 32.3%, 36.3% and 29.2% has also been achieved for the experiments on

Table 6: Summary of the segmentation results for VW acquired iris images

	Segmentation Error, E			
	UBIRIS.v2		**FRGC**	
	Sclera	***Iris***	***Sclera***	***Iris***
Proposed method (NN)	N/A	**1.90**	N/A	**1.84**
Proposed method (SVM)	N/A	**2.05**	N/A	**2.14**
Method 1 [4]	4.99	3.75	6.50	2.42
Method 2 [12]	N/A	3.49	N/A	3.30

N/A – Not Applicable

Table 7: Summary of the segmentation results for NIR acquired iris images

	Segmentation Error, E
	CASIA.v4-distance
	Iris
Proposed method (NN)	**1.13**
Proposed method (SVM)	**1.09**
Method 1 [4]	1.61
Method 2 [12]	1.71
Method 3 [10]	1.54

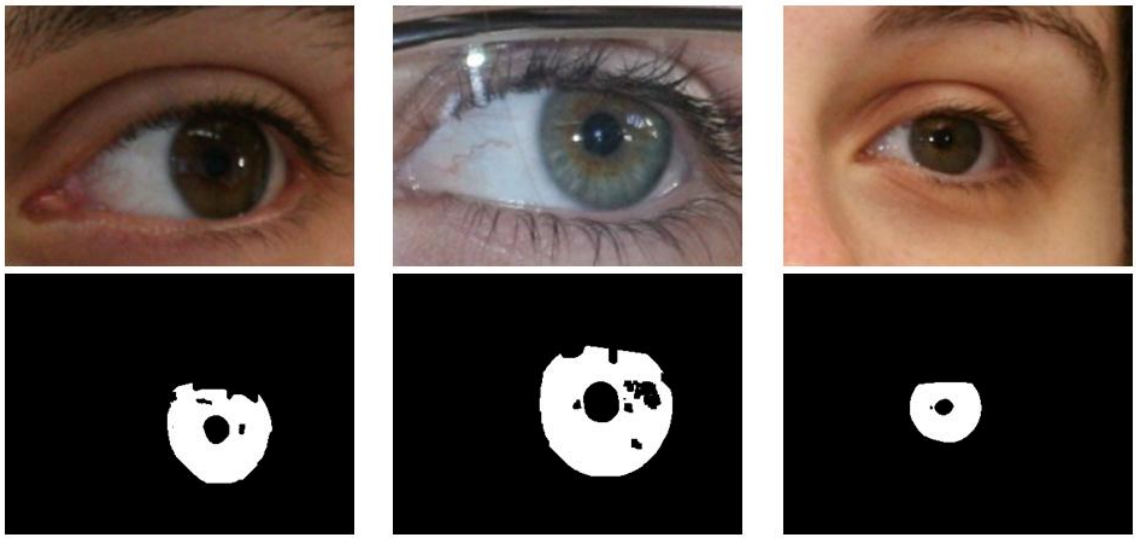

(a)

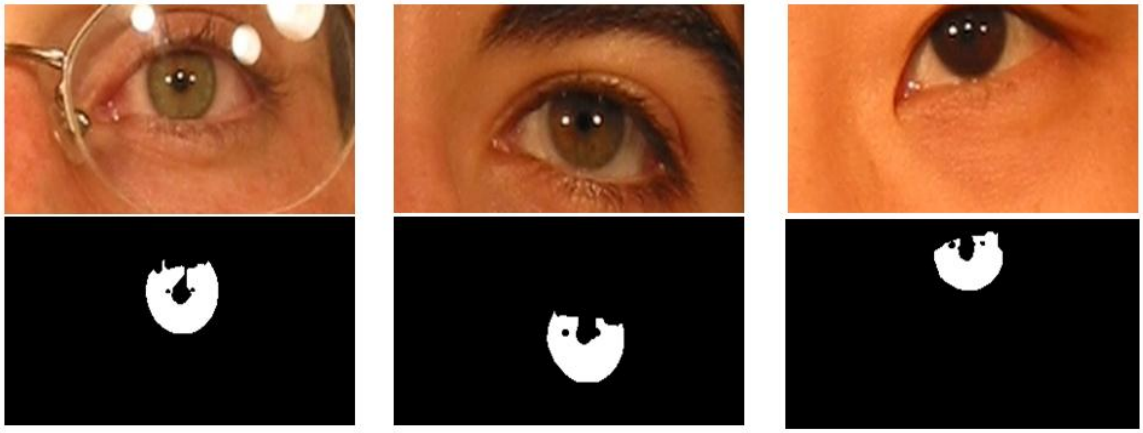

(b)

Fig. 16. Sample segmentation results from VW databases employed in experiments; (a) UBIRIS.v2, (b) FRGC.

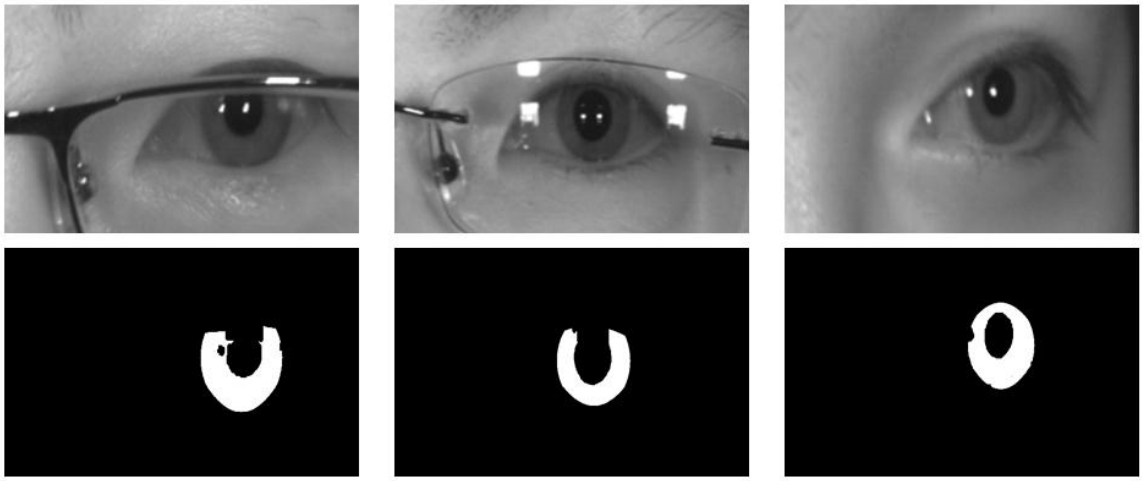

Fig. 17. Sample segmentation results from NIR database (CASIA.v4-distance) employed in experiments.

CASIA.v4-distance database, as compared to [4], [12], and [10], respectively. In general, the average improvements achieved by the proposed method on UBIRIS.v2, FRGC and CASIA.v4-distance databases are **47.5%**, **34.1%** and **32.6%**, respectively. Fig. 16 and 17 show some sample segmentation results produced by the proposed iris segmentation approach on the three publicly available databases as mentioned above.

3.2.2 Experiments on recognition (*R*)

Conventional iris imaging using NIR illumination has been shown to offer highly accurate performance for the personal identification [2], [7]-[10], [19], [33]-[34]. This could be attributed to the accurate segmentation and extraction of discriminative iris features in the controlled acquisition environment. On the contrary, distantly acquired iris images in real or unconstrained

VW illumination environments are often noisy which can result from defocus, motion blur, scale, pose changes and shadows. Therefore such images are often of degraded image quality and have questionable pieces of information for their usefulness in the human identification. As such, experiments described in this section investigate the usefulness of such distantly acquired face/iris images for reliable human recognition and also verification. The segmented iris images and the corresponding masks are normalized[††††] using the rubber sheet model [2]. The feature extraction on each of the segmented and normalized iris images is performed using 1D Log-Gabor filter [36]. The parameters of the 1D Log-Gabor, *i.e.*, center wavelength and SigmaOnf (σ_f/f_o), was estimated from the training images of the respective database and are as follows: UBIRIS.v2 (35/0.3), FRGC (20/0.5) and CASIA.v4 (20/0.25). Hamming distance is employed to compute the matching score between probe and gallery sets. The verification and identification performance on the independent test set from the three employed databases is illustrated from the receiver operating characteristics (ROC) and cumulative match characteristics (CMC), respectively in Fig. 18 and 19. The recognition results, for the images acquired from the NIR and VW illuminations, suggests that the proposed approach outperforms the other methods considered in this work. The results for the distantly acquired images using NIR illumination provide superior performance than those images acquired using VW illumination under unconstrained environments. It can also be observed that the recognition performance for the noisy images acquired using VW illumination is not adequate to be considered for high security or forensic applications. The conventional iris feature extraction strategies such as the one employed in this work may not able to effectively extract discriminative feature from the iris

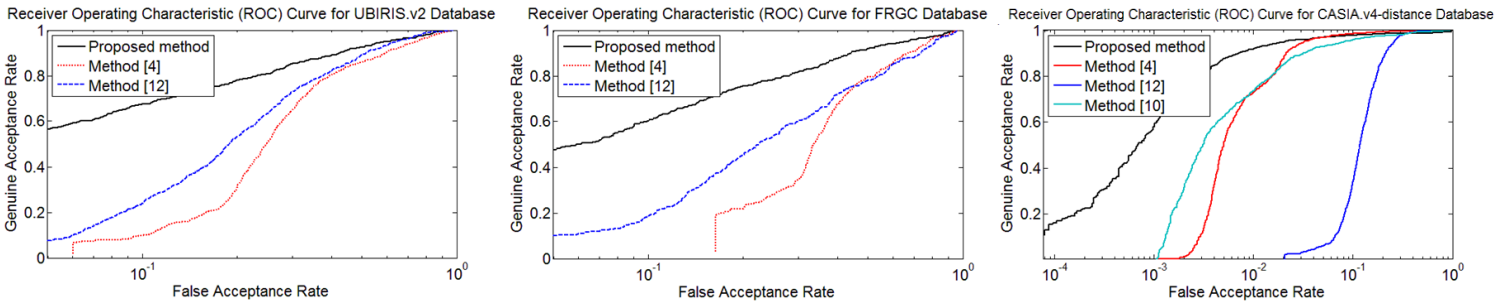

Fig. 18. ROC curves from the experiments using (a) UBIRIS.v2, (b) FRGC, and (c) CASIA.v4-distance database.

[††††] The normalized templates for UBIRIS.v2, FRGC and CASIA.v4 are of sizes of 512 × 64, 256 × 32 and 512 × 64, respectively.

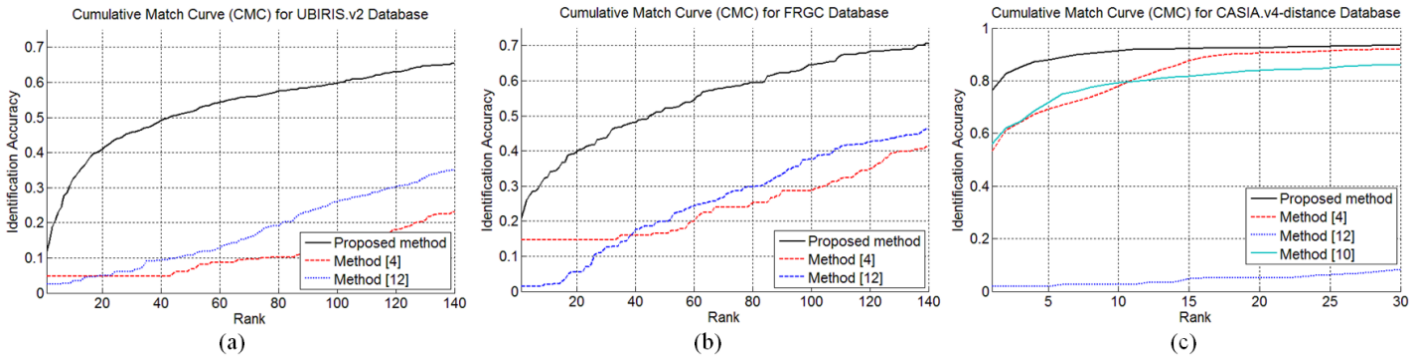

Fig. 19. CMC curves from the experiments using (a) UBIRIS.v2, (b) FRGC, and (c) CASIA.v4-distance database.

images acquired using VW illumination under unconstrained environments. The nature and the distribution of features which are observed in the normalized VW illumination iris images is quite unique and different than those from normalized images using acquired NIR illumination. Therefore the development of feature extraction and matching techniques which are tailored to the nature of the features, observed under VW illumination, can help to further improve the performance for the VW iris recognition and should pursued in the further work.

4. Discussion and Conclusions

This paper has detailed the development of a new approach for the completely automated iris segmentation using distantly acquired facial images. The iris recognition performance has also been evaluated to ascertain the usefulness/superiority of the correspondingly segmented iris images from the distantly acquired images. The main conclusions/contributions from of the work described in this paper can be summarized as follows:

1. A unified framework for completely automated iris segmentation using images acquired in *both* visible and NIR imaging is presented. The proposed approach exploits the higher order pixel relationship in a local region using Zernike moments and performs the pixel-based classification using trained NN/SVM classifier. In particular, the pixel-based classification addresses the problem of conventional segmentation approaches for segmenting images acquired at a distance and under unconstrained environments. Experimental results (Table 5 and Table 6) presented on three publicly available databases in section 3.2.1 illustrated superior performance than previously proposed approaches for the VW imaging iris segmentation. The presented results suggest

significant improvement in the average segmentation error by 47.5%, 34.1% and 32.6% over the previously proposed approaches.

2. The developed framework has incorporated robust post-classification processing operations which have been detailed in Section 2.2. These developed operations have been found to be highly efficient to mitigate the classification errors from the classification stage. These important steps are found not to be comprehensive in the previous approaches [4], [10]. When applying the developed post-classification processing to the classification results obtained using [4], the segmentation errors can be further improved by 34.7%, 10.3% and 25.5% for UBIRIS.v2, FRGC and CASIA.v4-distance databases, respectively. The presented results have not only confirmed the effectiveness of the developed techniques but also suggest potential adaptability of the developed techniques with other segmentation approaches to further refine the segmentation results.
3. Image enhancement using SSR has been employed in this paper to account for the illumination variation problem. SSR is a color constancy algorithm which helps to alleviate the influence of the varying illumination to the iris segmentation problem. Illumination variation is often significant in the images acquired under unconstrained environments. Such problem has also been discussed in previous approaches [4], [12], but there have not yet been any effort to address this problem.
4. In addition to the NN, we have presented the segmentation results of the proposed method obtained using SVM classifier. The NN classifier often suffer from the performance limitation due to the local minima problems and it requires rigorous training to ensure good classification performance. Therefore, an alternative classifier which requires least amount of training and provides competing or better performance is highly desirable. The SVM classifier was therefore evaluated in this paper and achieved competing performance to than those from NN classifier (Table 5 and 6). One of the possible reasons that SVM has not performed better than NN for iris classification (except for the case of CASIA.v4-distance database) could be due to the lack of adequate training samples (see Table 3). In general, all the segmentation results obtained using our method with NN/SVM classifier outperforms other state-of-the-art segmentation approaches considered in this paper.

5. Unlike previous efforts on visible imaging iris segmentation, this paper presented *iris recognition* performance from several publicly available databases. The proposed iris segmentation approach achieves superior performance (Section 3.2.2) for the iris recognition as compared to those from previously developed approaches. The experimental results from distantly acquired (noisy) iris images are not yet comparable to those from conventional iris recognition systems for commercial/civilian applications. However, these have high potential for surveillance and forensic applications as shown from the iris recognition results in this paper.

   The experiment results from the distantly acquired face/iris images using the developed iris segmentation approach are promising but require further efforts to exploit complimentary information for the human recognition. For example, fusion with other biometric modalities such as face or periocular features is expected to greatly improve the recognition performance and is suggested for further work. Previous work on periocular biometrics [23], [42] using the distantly acquired FRGC dataset has not attempted to exploit (ignored) iris features and our work has shown the usefulness of such iris features in the human recognition. Another possible approach to explore the performance improvement is to exploit the inconsistent/unstable bits in the iris code. The iris code produced as a quantization result of the filtered response for the noisy image is likely to be unstable due to the unconstrained imaging conditions. We believe that the performance from iris recognition-at-a-distance can be further improved by analyzing those unstable/inconsistent bits in the iris code. In this context recent efforts in [39]-[41] have shown promising results but for the iris code generated from the images NIR under imaging. The utility and applicability of these methods for the VW acquired images for the robust human verification/identification requires further investigation. Feature extraction based on orientation estimation [44], or multilobe differential filtering (MLDFs) [38] can hold some promises for extracting more discriminative VW iris features. However, due to the high degrees of freedom for configuring MLDFs, a thorough study is required to search for the best possible configurations which can effectively work for VW iris images and is suggested for further work.

Acknowledgments

We thankfully acknowledge the valuable comments and suggestions from the associate editor and the anonymous reviewers which have helped us to improve this paper. Authors thankfully

acknowledge SOCIA Lab (University of Beira Interior, Portugal), NIST (USA) and CASIA (Chinese Academy of Sciences' Institute of Automation, China) for their contributions to the databases employed in this work.

References

[1] K. Bowyer, K. Hollingsworth, and P. Flynn, "Image understanding for iris biometrics: A survey," *Image & Vision Computing*, vol. 110, no. 2, pp. 281–307, 2008.

[2] J. Daugman, "How iris recognition works," *IEEE Trans. Circuits Syst. Video Technol.*, vol. 14, no. 1, pp. 21–30, 2004.

[3] H. Proenca, S. Filipe, R. Santos, J. Oliveira, and L. Alexandre, "The UBIRIS.v2: A database of visible wavelength images captured on the move and at-a-distance," *IEEE Trans. Pattern Anal. Mach. Intell.*, vol. 32, no. 8, pp. 1529–1535, 2010.

[4] H. Proenca, "Iris recognition: On the segmentation of degraded images acquired in the visible Wavelength," *IEEE Trans. Pattern Anal. Mach. Intell.*, vol. 32, no. 8, pp. 1502–1516, 2010.

[5] N. Kourkoumelis and M. Tzaphlidou, "Medical safety issues concerning the use of incoherent infrared light in biometrics," *Ethics and Policy of Biometrics*, LNCS 6005, pp. 121–126, 2010.

[6] H. Proenca and L. Alexandre, "UBIRIS: A noisy iris image database," *Proc. ICIAP 2005, Intern. Conf. Image Analysis and Processing*, vol. 1, 2005.

[7] J. Daugman, "New methods in iris recognition," *IEEE Trans. Syst. Man Cybern. Part B Cybern.*, vol. 37, no. 5, pp. 1167–1175, 2007.

[8] Schuckers, N. Schmid, A. Abhyankar, V. Dorairaj, C. Boyce, and L. Hornak, "On techniques for angle compensation in nonideal iris recognition," *IEEE Trans. Syst. Man Cybern. Part B Cybern.*, vol. 37, no. 5, pp. 1176–1190, 2007.

[9] K. Miyazawa, K. Ito, T. Aoki, K. Kobayashi, and H. Nakajima, "An effective approach for iris recognition using phase-based image matching," *IEEE Trans. Pattern Anal. Mach. Intell.*, vol. 30, pp. 1741–1756, 2008.

[10] A. Kumar and A. Passi, "Comparison and combination of iris matchers for reliable personal authentication," *Pattern Recognit.*, vol. 43, no. 3, pp. 1016–1026, 2010.

[11] CASIA Iris Database version 3.0. http://www.cbsr.ia.ac.cn/english/IrisDatabase.asp.

[12] T. Tan, Z. He, and Z. Sun, "Efficient and robust segmentation of noisy iris images for non-cooperative iris recognition," *Image Vision Comput.*, vol. 28, no. 2, pp. 223–230, 2010.

[13] NICE.I - Noisy Iris Challenge Evaluation, Part I. http://nice1.di.ubi.pt/index.html.

[14] J. Shutler, "Complex Zernike moments," 8 2002. http://homepages.inf.ed.ac.uk/rbf/CVonline/LOCAL_COPIES/SHUTLER3/node11.html.

[15] K.-Y. Chang, "LANS Pattern Recognition Toolbox (MATLAB)." http://www.lans.ece.utexas.edu/~lans/index.shtml.

[16] Face Recognition Grand Challenge – Overview. http://www.nist.gov/itl/iad/ig/frgc.cfm

[17] C.-C. Chang and C.-J. Lin, "LIBSVM : a library for support vector machines," 2001. http://www.csie.ntu.edu.tw/~cjlin/libsvm.

[18] C.-W. Hsu, C.-C. Chang, and C.-J. Lin, "A practical guide to support vector classification," 2010. http://www.csie.ntu.edu.tw/~cjlin/papers/guide/guide.pdf.

[19] Z. He, T. Tan, Z. Sun, and X. Qiu, "Toward accurate and fast iris segmentation for iris biometrics," *IEEE Trans. Pattern Anal. Mach. Intell.*, vol. 31, no. 9, pp. 1670–1684, 2009.

[20] NICE:II - Noisy Iris Challenge Evaluation, Part II. http://nice2.di.ubi.pt/.

[21] P. Phillips, P. Flynn, T. Scruggs, K. Bowyer, J. Chang, K. Hoffman, J. Marques, J. Min, and W.Worek, "Overview of the face recognition grand challenge," *in Computer Vision and Pattern Recognition, 2005. CVPR 2005*. 2005.

[22] G. Bradski, "The OpenCV Library," Dr. Dobb's Journal of Software Tools, 2000.

[23] U. Park, R. R. Jillela, A. Ross, and A. K. Jain, "Periocular biometrics in the visible spectrum," *IEEE Trans. Info. Forensics & Security*, vol. 6, no. 1, pp. 96–106, 2011.

[24] C.-H. Teh, and R.T. Chin, "On image analysis by the methods of moments," *IEEE Trans. Pattern Anal. Mach. Intell.*, vol.10, no.4, pp.496-513, 1988.
[25] A. Khotanzad and Y. H. Hong, "Invariant image recognition by Zernike moments," *IEEE Trans. Pattern Anal. Mach. Intell.*, vol.12, no.5, pp.489-497, 1990.
[26] M.T. Hagan and M.B. Menhaj, "Training feedforward networks with the Marquardt algorithm," *IEEE Trans. Neural Networks*, vol.5, no.6, pp.989-993, 1994.
[27] J. Wang, P. Neskovic, and L. N. Cooper, "Training Data Selection for Support Vector Machines," *in Advances in Natural Computation (ICNC)*, L. Wang, K. Chen, Y. S. Ong (*Eds.*), LNCS 3610, pp. 554-564, 2005.
[28] D. H. Brainard and B. A. Wandell, "Analysis of the retinex theory of color vision," *J. Opt. Soc. Am. A:*, vol.3, no. 10, pp.1651-1661, 1986.
[29] V. Štruc and N. Pavešić, "Performance Evaluation of Photometric Normalization Techniques for Illumination Invariant Face Recognition," *in Advances in Face Image Analysis: Techniques and Technologies*, Y.J. Zhang (*Ed.*), IGI Global.
[30] V. Štruc and N. Pavešić, "Gabor-Based Kernel Partial-Least-Squares Discrimination Features for Face Recognition," *Informatica (Vilnius)*, vol. 20, no. 1, pp.115–138, 2009.
[31] Biometrics Ideal Test. http://biometrics.idealtest.org/dbDetailForUser.do?id=4
[32] R.C. Gonzalez, R.E. Woods and S.L. Eddins, *Digital Image Processing Using Matlab*, Prentice Hall, pp.384-392, 2003.
[33] J. Zuo and N.A. Schmid, "On a Methodology for Robust Segmentation of Nonideal Iris Images," *IEEE Trans. Sys. Man Cybern., Part B Cybern.*, vol.40, no.3, pp.703-718, 2010.
[34] L. Ma, T. Tan, Y. Wang, and D. Zhang, "Personal identification based on iris texture analysis," *IEEE Trans. Pattern Anal. Mach. Intell.*, vol.25, no.12, pp. 1519- 1533, 2003.
[35] ISO/IEC 19794-6:2005. Information technology -- Biometric data interchange formats -- Part 6: Iris image data.
[36] L. Masek and P. Kovesi, *MATLAB Source Code for a Biometric Identification System Based on Iris Patterns*, The School of Computer Science and Software Engineering, The University of Western Australia. 2003. http://www.csse.uwa.edu.au/~pk/studentprojects/libor/index.html
[37] C.-W. Tan and A. Kumar, "Automated segmentation of iris images using visible wavelength face images," *Proc. CVPR 2011*, pp. 9-14, Colorado Springs, CVPRW'11, June 2011.
[38] Z. Sun and T. Tan, "Ordinal Measures for Iris Recognition," *IEEE Trans. Pattern Anal. Mach. Intell.*, vol.31, no.12, pp.2211-2226, 2009.
[39] K. P. Hollingsworth, K.W. Bowyer, and P.J. Flynn, "The Best Bits in an Iris Code," *IEEE Trans. Pattern Anal. Mach. Intell.*, vol.31, no.6, pp.964-973, 2009.
[40] K. P. Hollingsworth, K.W. Bowyer, and P.J. Flynn, "Using fragile bit coincidence to improve iris recognition," *Proc. BTAS 2009*, vol., pp.1-6, 28-30 Sept. 2009.
[41] K. P. Hollingsworth, K.W. Bowyer, and P.J. Flynn, "Improved Iris Recognition Through Fusion of Hamming Distance and Fragile Bit Distance," *IEEE Trans. Pattern Anal. Mach. Intell.*, (available online).
[42] D. L. Woodard, S. Pundlik, P. Miller, R. Jillela, and A. Ross, "On the Fusion of Periocular and Iris Biometrics in Non-ideal Imagery," *Proc. Intl. Conf. Pattern Recognition*, ICPR 2010, Istanbul (Turkey), pp.201-204, 23-26 Aug. 2010.
[43] Ground truth masks and program codes for iris the segmentation http://www.comp.polyu.edu.hk/~csajaykr/myhome/research/paper11.zip
[44] A. Kumar, Tak Shing Chan, Chun-Wei Tan, "Human identification from at-a-distance face images using sparse representation of local iris features," *Proc. ICB 2012*, New Delhi, India, Mar. 2012.
[45] S. Venugopalan, U. Prasad, K. Harun, K. Neblett, D. Toomey, J. Heyman, and M. Savvides , "Long Range Iris Acquisition System for Stationary and Mobile Subjects," *Proc. IJCB 2011*, Washington DC, Oct, 2011.